International Conference on Mathematics, Computational Methods & Reactor Physics (M&C 2009)
Saratoga Springs, New York, May 3-7, 2009, on CD-ROM, American Nuclear Society, LaGrange Park, IL (2009)

MODELING OF RADIATION TRANSPORT IN COUPLED ATMOSPHERE-SNOW-ICE-OCEAN SYSTEMS

Knut Stamnes
Stevens Institute of Technology
Hoboken, NJ 07030
kstamnes@stevens.edu

Børge Hamre and Jakob J. Stamnes
Department of Physics and Technology
University of Bergen
Allégaten 55, Bergen, Norway
Borge.Hamre@ift.uib.no

Gennady Ryzhikov and Marina Biryulina
Geminali AS
P.O. Box 165 Lilleaker
0216 Oslo, Norway
Gennady.Ryzhikov@ift.uib.no

ABSTRACT

A radiative transfer model for coupled atmosphere-snow-ice-ocean systems is used to develop accurate and efficient tools for computing the BRDF of sea ice for a wide range of situations occurring in nature.

Key Words: Radiation transport, snow, sea ice, ocean, BRDF

1. INTRODUCTION

Brief description of coupled atmosphere-surface radiative transfer models. We consider an atmosphere-ice medium consisting of two adjacent horizontal slabs with different refractive indices. In each slab the inherent optical properties (IOPs) vary in the vertical direction only, and the diffuse radiance distribution $I(\tau,\mu,\phi)$ can be described by

$$\mu\frac{dI(\tau,\mu,\phi)}{d\tau} = I(\tau,\mu,\phi) - \frac{\omega}{4\pi}\int_0^{2\pi} d\phi' \int_{-1}^{1} p(\tau,\mu',\phi';\mu,\phi)I(\tau,\mu',\phi')d\mu' - S^*(\tau,\mu',\phi'). \qquad (1)$$

Here $\omega = a/(a+b)$ is the single-scattering albedo, a and b being the absorption and scattering coefficients, respectively, $p(\tau,\mu',\phi';\mu,\phi) = p(\cos\Theta)$ is the scattering phase function, which is normalized such that $\int_{4\pi}(p(\cos\Theta)/4\pi)d\omega = 1$, $\mu' = \cos\theta'$, $\mu = \cos\theta$, θ' and θ being the polar angles of the radiance before a scattering event and the observed radiance, respectively, ϕ' and ϕ being the corresponding azimuth angles. The scattering angle Θ and the polar and azimuth angles are related by $\cos\Theta = \cos\theta\ \cos\theta' + \sin\theta'\ \sin\theta\ \cos(\phi'-\phi)$. The optical depth τ increases

downward with depth from $\tau = 0$ at the top of the atmosphere. The single-scattering source term $S^*(\tau, \mu', \phi')$ in Eq. (1) in the air is

$$S^*_{air}(\tau, \mu, \phi) = \frac{\omega(\tau)F_s}{4\pi}[p(\tau, -\mu_0, \phi_0; \mu, \phi)e^{-\tau/\mu_0} + \rho_s\, p(\tau, \mu_0, \phi_0; \mu, \phi)e^{-(2\tau_a-\tau)/\mu_0}] \qquad (2)$$

where τ_a is the vertical optical depth of the air, $\rho_s \equiv \rho_s(-\mu_0; m_{rel})$ is the reflectance from the air-ice interface, $\mu_0 = \cos\theta_0$, where θ_0 is the solar zenith angle, and $m_{rel} = n_{ice}/n_{air} > 1$ is the real part of the refractive index of ice relative to that of air. The first term on the right hand side of Eq. (2) is due to first-order scattering of the attenuated incident solar beam of irradiance F_s (normal to the beam) while the second term is due to first-order scattering of the attenuated incident beam that is specularly reflected from the air-ice interface. In the ice the single-scattering source term consists of the attenuated incident beam that is refracted through the interface, *i.e.*

$$S^*_{ice}(\tau, \mu, \phi) = \frac{\omega(\tau)F_s}{4\pi}\frac{\mu_0}{\mu_{0n}}\mathcal{T}(-\mu_0; m_{rel})p(\tau, -\mu_{0n}, \phi_0; \mu, \phi)e^{-\tau_a/\mu_0}e^{-(\tau-\tau_a)/\mu_{0n}} \qquad (3)$$

where $\mathcal{T}(-\mu_0; m_{rel})$ is the transmittance through the interface, and μ_{0n} is the cosine of the polar angle θ_{0n} in the ice, which is related to $\theta_0 = \arccos\mu_0$ by Snell's law. We may isolate the azimuth dependence by expanding the scattering phase function in *Legendre polynomials*

$$p(\cos\Theta) \;=\; p(\mu', \phi'; \mu, \phi) \;=\; \sum_{m=0}^{2N-1}(2 - \delta_{0,m})p^m(\mu', \mu)\;\cos m(\phi' - \phi) \qquad (4)$$

where $\delta_{0,m}$ is the Kronecker delta function, *i.e.* $\delta_{0,m} = 1$ for $m = 0$ and $\delta_{0,m} = 0$ for $m \neq 0$, and

$$p^m(\mu', \mu) = \sum_{l=m}^{2N-1}(2l + 1)\chi_l\Lambda^m_l(\mu')\Lambda^m_l(\mu); \quad \Lambda^m_l(\mu) \equiv \sqrt{\frac{(l-m)!}{(l+m)!}}P^m_l(\mu). \qquad (5)$$

Here χ_l is an expansion coefficient and $P^m_l(\mu)$ is the associated Legendre polynomial. Expanding the radiance in a similar way

$$I(\tau,\mu, \phi) = \sum_{m=0}^{2N-1} I^m(\tau,\mu)\;\cos m(\phi - \phi_0) \qquad (6)$$

where ϕ_0 is the azimuth angle of the incident light, we find that each Fourier expansion coefficient satisfies (see Refs. [1–4] for details)

$$\frac{dI^m(\tau, \mu)}{d\tau} = I^m(\tau, \mu) - \frac{\omega(\tau)}{2}\int_{-1}^{1} p^m(\tau, \mu', \mu)\, I^m(\tau, \mu)\, d\mu - S^{*m}(\tau, \mu) \qquad (7)$$

where $m = 0, 1, 2, \ldots, 2N - 1$ and $p^m(\mu', \mu)$ is given by Eq. (5). To solve this equation for the coupled air-ice system we need to take into account the boundary conditions at the top of the atmosphere and at the bottom of the ice and also the reflection and transmission at the air-ice interface. In addition the radiance must satisfy continuity conditions at each interface between horizontal layers with different optical properties in the air and the ice.

In the discrete ordinate approximation we approximate the integral in Eq. (7) by a quadrature sum consisting of $2N_1$ 'streams' in the air (N_1 in each hemisphere). At the air-ice interface the N_1 streams used to represent the radiance in the downward hemisphere in the air refract through the interface into the ice. In the ice we use $N_2 > N_1$ streams (in each hemisphere), where the additional $(N_2 - N_1)$ streams are used to represent the radiance in the region of total reflection. Use of Gaussian quadrature guarantees that energy is conserved in the discrete ordinate approximation (see Ref. [4] for details). Adequate accuracy is obtained by using a sufficiently large number of streams, which to a large extent depends on the asymmetry of the scattering phase function. In practice, we double the number of streams until the results converge. In the calculations reported here we set the number of streams high enough to satisfy our accuracy requirements.

The original model was developed for a coupled atmosphere-ocean (CAO) system [1], based on the well-tested discrete-ordinate radiative transfer (DISORT) method for a medium having a constant refractive index [2, 3]. This CAO-DISORT model was tested against several other models [5], notably against an accurate Monte Carlo model [6], and was extended to apply to a coupled atmosphere-snow-ice-ocean (CASIO) system [7]. Applications of the CASIO-DISORT model to field data for first-year sea ice [9, 10] resulted in updated and improved sea ice IOPs that are used in this work.

Overview of BRDF computational approach. We used CASIO-DISORT to develop tools for accurate and efficient computation of the sea ice BRDF. To quantify it, we need the backscattered radiance distribution as a function of the polar angles θ_0 and θ of incidence and observation, respectively, as well as the corresponding azimuth-difference angle $\Delta\phi = \phi - \phi_0$. According to Eq. (6), the radiance distribution can be expressed as a Fourier cosine series in which the expansion coefficients $I^m(\tau, \mu)$ depend on the polar angles θ_0 and θ as well as on the sea ice IOPs. Each expansion coefficient satisfies Eq. (7), which is readily solved by the DISORT method to provide $I^m(\tau, \mu)$, and Eq. (6) then yields the complete angular distribution of the radiance as a function of θ_0, θ, and $\Delta\phi$. With no atmosphere assumed to be present, so that $S^*_{air}(\tau, \mu, \phi) = 0$ [Eq. (2)], we tabulated the expansion coefficients $I^m(\tau, \mu)$ for a number of θ_0 values (solar zenith angles), θ values (view angles), and sea ice IOPs and stored the results in a set of lookup tables (LUTs). Based on prior experience [11, 12], we selected an appropriate grid structure in θ_0 and θ, as well as in sea ice IOPs so that interpolation in the LUTs would allow computation of the backscattered radiance distribution and thus the BRDF with desired accuracy.

To create lookup tables for the sea ice BRDF to be used for interpolation, we assumed no atmosphere to be present, the ice to be floating on water with a known albedo A_w, and the IOPs of a slab of sea ice to be characterized by its optical thickness τ, its single-scattering albedo ω, and its asymmetry parameter g. Then we used CASIO-DISORT to tabulate the expansion coefficients $I^m(\tau, \omega, g, \mu_0, \mu, A_w)$, which determine the sea ice BRDF as a function of τ, ω, g, μ_0, μ, and A_w. We also created a tool for computing sea ice IOPs (τ, ω, and g) for any specific wavelength desired (see §2) from sea ice physical parameters: real and imaginary parts of the sea ice refractive index, brine pocket concentration and effective size, air bubble concentration and effective size, volume fraction and absorption coefficient of ice impurities, asymmetry parameters for scattering by brine pockets and air bubbles, and sea ice thickness. For each of the six

parameters listed above ($\tau, \omega, g, \mu_0, \mu, A_w$) we determined an appropriate range and a suitable grid to enable accurate interpolation of $I^m(\tau, \omega, g, \mu_0, \mu, A_w)$ in the LUTs (see §4). This approach enabled a reliable computation of the wavelength-dependent BRDF as a function of sea ice IOPs. The BRDF for snow can easily be included as a "cloud on top of the sea ice" layer in the DISORT version 2 (DISORT2) radiative transfer model [3]. Thus, all we need is a tool for computing the IOPs (τ, ω, and g) for snow from snow physical parameters (snow effective grain size, density, and impurity concentration) for the specific wavelengths desired (see §2).

2. PARAMETRIZATION OF INHERENT OPTICAL PROPERTIES (IOPs)

Snow and sea ice IOPs – General Approach. For wavelengths $\lambda \leq 1.2$ μm, the absorption efficiency Q_a and the scattering efficiency Q_b for snow grains, sea ice brine inclusions, and sea ice air bubbles may be derived from geometrical optics as [8, 9]

$$Q'_a(r) = \frac{16\pi r}{3\lambda}\frac{k}{n}[n^3 - (n^2-1)^{(3/2)}]; \qquad Q'_b(r) = 2 \tag{8}$$

where r is the effective particle radius, and n and k are the real and imaginary parts of the refractive index, respectively, for the particle type in question.

Extension of particle IOP parameterization to longer wavelengths. The parameterizations of the IOPs for snow grains, and sea ice inclusions (brine pockets and air bubbles) provided by Hamre et al. [9] are valid for wavelengths shorter than about 1.2 μm. To extend the validity to near infrared wavelengths, we used the following modified parameterizations, which are based in part on fits to results from Mie calculations:

$$Q_a = 0.94[1 - \exp(Q'_a/0.94)]; \qquad Q_b = 2 - Q_a; \qquad g = g_0^{(1-Q_a)^{0.6}} \tag{9}$$

where Q'_a is given by Eq. (8), and g is the asymmetry parameter of the scattering phase function for large particles ($r > \sim 50$ μm), g_0 being the asymmetry parameter for non-absorbing particles ($k = 0$). The asymmetry parameter g can be assumed not to depend on the wavelength and set equal to 0.85, 0.89, and 0.997 for air bubbles, snow grains, and brine pockets, respectively. For a medium consisting of several absorbing and scattering constituents the total absorption and scattering efficiencies are just the sum of those due to the separate constituents. The optical thickness τ and single-scattering albedo ω for a slab of thickness h become

$$\tau = \pi r^2 N h(Q_a + Q_b); \qquad \omega = \frac{Q_b}{Q_a + Q_b} \tag{10}$$

where N is the total number of particles per unit volume, and Q_a and Q_b are the total absorption and scattering efficiencies. In highly scattering media such as snow and sea ice we may use the Henyey-Greenstein scattering phase function

$$p(\cos\Theta) = \frac{1-g^2}{(1+g^2-2g\cos\Theta)^{3/2}} \tag{11}$$

where g is the asymmetry parameter ($-1 < g < 1$) and Θ the scattering angle, to describe the angular scattering behavior. The modified parameterizations, which are represented by the

dash-dot curves in Fig. 1, are seen to work well for wavelengths shorter than about 2.8 μm, but to deviate significantly from predictions by Mie theory for longer wavelengths. Thus, for wavelengths longer than 2.8 μm it may be preferable to use results from Mie theory. Note that for wavelengths shorter than 2.8 μm, where the parameterizations work well, the variations in n and k are large. Thus, one would expect these parameterizations to be representative for most types of large particles.

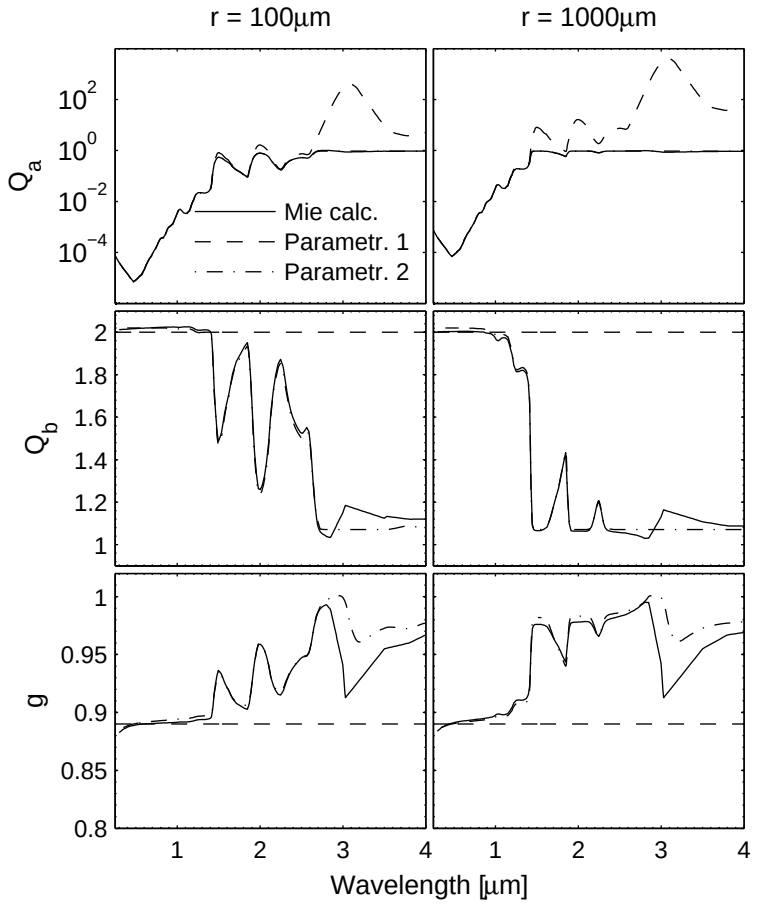

Figure 1. Comparisons of IOPs calculated using Mie theory with those obtained using Parameterization 1, which is valid for wavelengths shorter than about 1.2 μm [9], and Parameterization 2, which is valid also in the near infrared.

Impurities, air bubbles, and brine pockets. If the volume fraction of impurities within a snow grain or brine pocket is not too large, which is the case for typical situations occurring in nature, scattering by impurities can be ignored, so that their effects can be included by simply adding the imaginary part k_m of the refractive index for impurities to k in Eq. (8). For typical impurities in snow and ice, the wavelength dependence of k_m can be parameterized as

$$k_m = k_m(\lambda_0)\,(\lambda_0/\lambda)^\eta \tag{12}$$

where η typically has values between 2 and 5, and $k_m(440\ \mathrm{nm})$ has values between 5×10^{-3} and 5×10^{-2} (roughly).

For snow, the number of snow grain particles per unit volume is $N = \frac{1}{\frac{4}{3}\pi r^3}\frac{\rho_s}{\rho_i}$, where r is the effective particle radius, while ρ_s and ρ_i are the densities of snow and pure ice, respectively. The optical thickness and the single-scattering albedo can be calculated from Eqs. (10) and (9), using the refractive indices of pure ice [13] and impurities [Eq. (12)]. We assumed that sea ice consists of pure ice with embedded brine pockets, air bubbles, and impurities. To include the effects of the embedded components, we first calculated the absorption coefficient a for sea ice

$$a = \pi r_{br}^2 N_{br} Q_{a,br} + \left[1 - \frac{4}{3}\pi r_{br}^3 N_{br} - \frac{4}{3}\pi r_{bu}^3 N_{bu}\right] \frac{4\pi(k_i + V_m k_m)}{\lambda} \tag{13}$$

where V_m is the volume fraction of impurities, N_{br} and N_{bu} are the number concentrations of brine pockets and air bubbles, respectively, r_{br} and r_{bu} are the corresponding effective radii, and $Q_{a,br}$ is the absorption efficiency for brine pockets. The two terms on the right side of Eq. (13) represent the absorption coefficients of brine pockets and surrounding ice (including impurities), respectively. In Eq. (13), we have used the general relation $a = 4\pi k/\lambda$, λ being the wavelength in vacuum, and the expression inside the square brackets is the volume fraction of the ice surrounding all brine pockets and bubbles.

The air bubbles were assumed to be non-absorbing ($Q_{a,bu}$ = 0), and the impurities were assumed to be uniformly distributed in the ice with k_i and k_m being the imaginary parts of the refractive indices for pure ice and impurities, respectively. For brine pockets, which are in the liquid phase, the refractive index of sea water was used. The volume fraction V_m of impurities typically lies in the range between 1×10^{-7} and 1×10^{-5}. The scattering coefficient b of sea ice is given by

$$b = b_{br} + b_{bu}; \quad b_{br} = \pi r_{br}^2 N_{br} Q_{b,br}; \quad b_{bu} = \pi r_{bu}^2 N_{bu} Q_{b,bu} \tag{14}$$

where b_{br} and b_{bu} are the scattering coefficients for brine pockets and air bubbles, respectively, and $Q_{b,br}$ and $Q_{b,bu}$ are the corresponding scattering efficiencies. Here we have ignored the scattering coefficient for pure sea ice because it is very small compared to either b_{br} or b_{bu}. The optical thickness τ, the single-scattering albedo ω, and the asymmetry parameter g for sea ice now become

$$\tau = (a+b)h; \qquad \omega = \frac{b}{a+b}; \qquad g = \frac{b_{br}g_{br} + b_{bu}g_{bu}}{b_{br} + b_{bu}}. \tag{15}$$

Reduced foward scattering transformations. If we assume the reduced scattering coefficient $s = b(1-g)$ to remain constant as g is reduced from a value close to unity to $g_{max} < 1$, the computed BRDF values will be invariant under the following transformations:

$$g' = g_{max}; \qquad \tau' = (a+b')h; \qquad b' = \frac{(1-g)b}{1-g_{max}}; \qquad \omega' = \frac{b'}{a+b'}. \tag{16}$$

These transformations effectively assume that some of the forward scattered light is not scattered at all but retained in the incoming beam. Hence, the resulting scattering phase function becomes less anisotropic, and the asymmetry parameter smaller. Figure 2 shows that the merit of these

transformations is to provide a smooth variation of the radiance versus the polar angle of observation for a reasonable number of discrete-ordinate streams, which in this computation was 52 in the air and 88 in the ice. To obtain the same accuracy without invoking the reduced forward scattering transformations in Eqs. (16) would require a doubling of the number of streams, which would be quite time consuming.

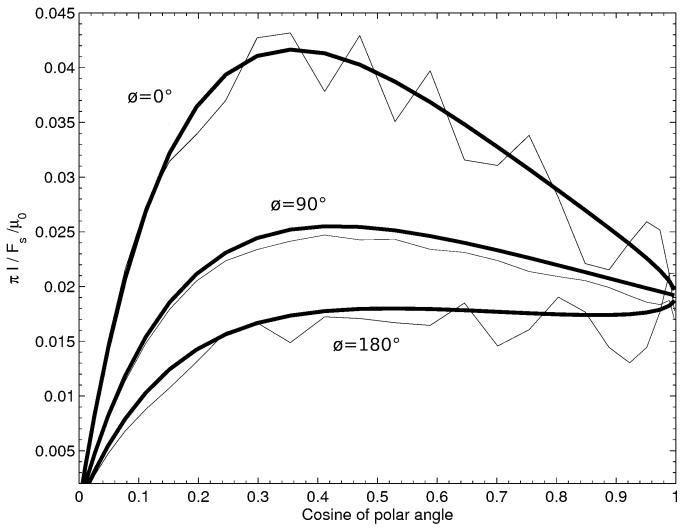

Figure 2. Comparisons of radiance computations done with (thick lines) and without (thin lines) use of the reduced forward scattering transformations for a slab of ice of thickness $h = 1$ m. Here g_{max} was set to 0.9, which for $\tau = 500$ ($b = 490$ m^{-1} and $a = 10$ m^{-1}) and $g = 0.99$, gives $\tau' = 59$ and $1 - \omega' = 0.17$.

3. ADDING SNOW AND A SPECULAR COMPONENT

To include snow on the ice we used DISORT2 [3], which allows for a BRDF to be used as a lower boundary condition at the bottom of the atmosphere. Also, we modified DISORT2 to accept Fourier expansion coefficients for the BDRF as input rather than the BRDF itself, and verified that using BRDF expansion coefficients as input gives the same answer as using the BRDF itself, but with a computation time reduction factor of about 60.

The BRDF computed by CASIO-DISORT or retrieved from the LUTs contains diffuse light only. Thus, it pertains to light that has been refracted into the sea ice, and then backscattered out of the ice due to multiple scattering inside it. But it does not include the direct component of the incident light that undergoes specular reflection at the air-ice interface. The total BRDF for sea ice, denoted by $\rho(\theta_0, \theta, \Delta\phi)$, can be split up into its diffuse and specular components [4]

$$\rho(\theta_0, \theta, \Delta\phi) = \frac{I^{dif}(\theta_0, \theta, \Delta\phi)}{F_s \cos\theta_0} + \frac{I^{spc}(\theta_0, \theta, \Delta\phi)}{F_s \cos\theta_0}.$$

Here θ_0 and θ are the polar angles of incidence and observation, F_s is the incident irradiance (normal to the beam), and $I^{dif}(\theta_0, \theta, \Delta\phi)$ and $I^{spc}(\theta_0, \theta, \Delta\phi)$ stand for the diffuse and specular

components of the backscattered light, respectively. For a perfectly smooth air-ice interface, $I^{spc}(\theta_0, \theta, \Delta\phi)$ would have a value different from zero only for $\theta = \theta_0$ and $\Delta\phi = \pi$. But because sea ice surfaces are not perfectly smooth, we approximated the specular reflection component with a Gaussian beam around the specular direction by setting

$$I^{spc}(\theta_0, \theta, \Delta\phi) \approx A(\theta_0) I^{Gauss}(\theta_0, \theta, \Delta\phi) \tag{17}$$

where $A(\theta_0)$ is a normalization constant. To determine $A(\theta_0)$ we considered the specularly reflected irradiance, which can be written as (see pages 136 and 319 in Ref. [4])

$$F^{spc}(\theta_0) = \rho_F(\theta_0) F_s \cos\theta_0 \tag{18}$$

where $\rho_F(\theta_0)$ is the reflectance given by Fresnel's equation (see Eq. (E.18), page 509 in Ref. [4]), and required that the albedo (or flux reflectance) for the Gaussian beam (assumed to be caused by surface roughness) be the same as the specularly reflected irradiance:

$$A(\theta_0) = \frac{\rho_F(\theta_0) F_s \cos\theta_0}{\int_{2\pi} I^{Gauss}(\theta_0, \theta, \Delta\phi) \cos\theta d\omega}. \tag{19}$$

Thus, the total BRDF [Eq. (17)] became

$$\rho(\theta_0, \theta, \Delta\phi) = \frac{I^{dif}(\theta_0, \theta, \Delta\phi)}{F_s \cos\theta_0} + \frac{\rho_F(\theta_0) I^{Gauss}(\theta_0, \theta, \Delta\phi)}{\int_{2\pi} I^{Gauss}(\theta_0, \theta, \Delta\phi) \cos\theta d\omega} \tag{20}$$

and the specular component of the BRDF [second term in Eq. (20)] could be used in DISORT2 in the usual manner by expanding it in a Fourier cosine series, computing the Fourier expansion coefficients, and finally computing the BRDF for the combined snow-sea ice system.

4. TESTING AND EVALUATION OF THE BDRF TOOL

Lookup tables for bare sea ice BRDF. As mentioned previously, CASIO-DISORT was used to compute the Fourier expansion coefficients in Eq. (6), which provides the BRDF for given directions of illumination and observation, sea ice IOP values, and ocean albedo values. These expansion coefficients were computed and stored in LUTs for ranges likely to be encountered in nature of ocean albedo A_w, co-asymmetry parameter $1 - g$ for sea ice, optical thickness τ^* of the sea ice layer, single-scattering co-albedo $1 - \omega$ for sea ice, as well as for a range of polar angles θ_0 of illumination and polar angles θ of observation. Comparisons of interpolated (ISBRDF) BRDF values with directly calculated (CASIO-DISORT) BRDF values for sea ice show that the accuracy of the interpolated values is within 1.5%.

Current capabilities and possible limitations. The accuracy of the IOPs becomes questionable for wavelengths longer than about 2.8 μm in snow and for wavelengths longer than 1.4 μm in ice. This is due to very high absorption, which leads to very little diffuse backscattered light. Three sets of LUTs were made that contain Fourier expansion coefficients for the following sea ice IOP ranges: **LUT-1 (thick ice:** $10 < \tau < 2000$**), LUT-2 (thin ice:** $0.01 < \tau < 10$**), LUT-3 (pure ice:** $0.01 < \tau < 2$**).**

These ranges cover most sea ice types, thicknesses, and wavelengths with the following exception. For wavelengths longer than about 1.3 μm, the maximum values of τ and $(1 - \omega)$ in

the LUTs may be exceeded. However, at these wavelengths the BRDF $[I/F_s \cos\theta_0]$ takes values on the order of 10^{-3}, which means that the backscattered radiance is only a fraction of a percent of that backscattered at 0.5 μm, and also smaller than the specularly reflected radiance at all wavelengths. Whenever τ or $(1-\omega)$ exceeds the maximum range in the LUTs, we set it equal to its maximum value, which would lead to negligible errors, because the BRDF is dominated by the specular component. A constant value equal to 1.31 for the real part of the refractive index of the sea ice was used in the CASIO-DISORT computations of the Fourier expansion coefficients stored in the LUTs. A plane sea ice surface was assumed, but the limitation implied by this assumption was addressed by adding a specularly reflected Gaussian beam component as described in §3. Note that **LUT-1** and **LUT-2** are similar except that the range of optical depths was extended in **LUT-2** to cover values between 0.01 and 10. **LUT-3** was added to cover pure ice with no air bubble or brine pocket inclusions. **LUT-3** is needed because the asymmetry parameters and the single scattering albedo values differ significantly from pure ice to normal sea ice. Thus, **LUT-1** and **LUT-2** do not contain the appropriate ranges for $(1-\omega)$ and $(1-g)$ encountered in pure ice.

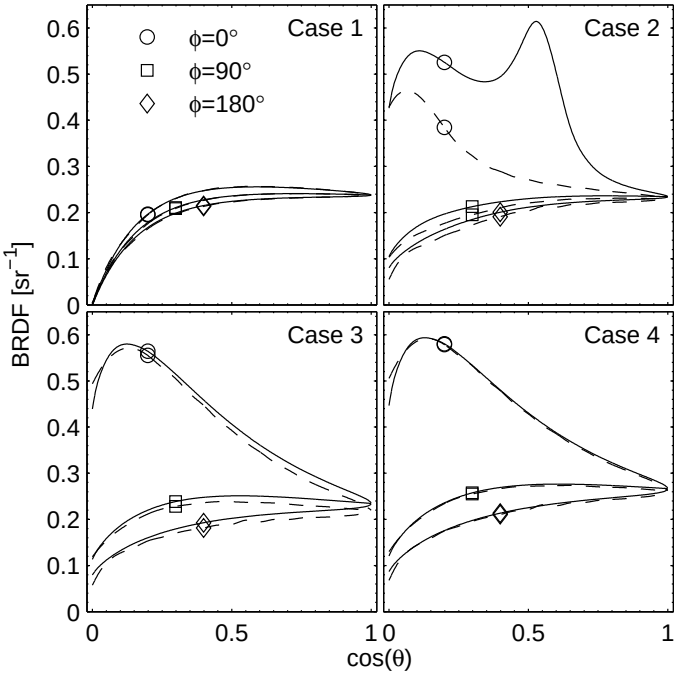

Figure 3. Comparisons between BRDFs computed with CASIO-DISORT (solid lines) and the ISBRDF package (broken lines) without specular reflection, so that the ISBRDF computations only include diffusely backscattered light. Case 1, 2, 3, and 4 represent 0, 1, 10, and 1000 mm of snow on top of the sea ice. Inputs used in the calculations: $\mu_0 = 0.55$; $g = 0.88$, $a + b = 500$ m^{-1}, $1-\omega = 3.5 \times 10^{-5}$ for snow; $g = 0.9724$, $\tau = 4.081 \times 10^2$, $1-\omega = 8.326 \times 10^{-5}$ for ice; $A_w = 0$.

Testing the BRDF for bare and snow-covered sea ice. Figure 3 shows a comparison between BRDF results produced by CAO-DISORT and the new ISBRDF tool without the air-ice interface specular reflection component included in the ISBRDF. As expected, the agreement is good for bare sea ice (Case 1). Also, the agreement is good for ice covered with a thick snow layer (Case 3

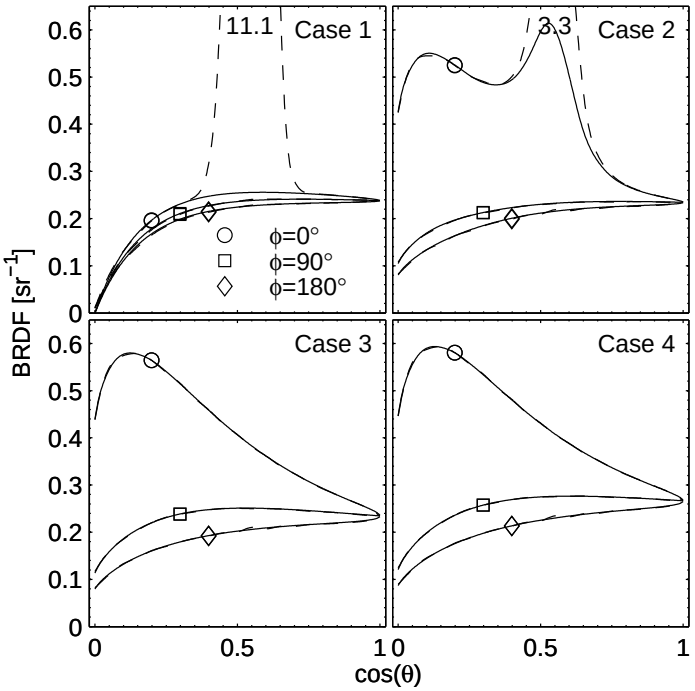

Figure 4. Same as Fig. 3 but now with the Gaussian specular reflection component (FWHM = 5°) included in ISBRDF. The numbers written on the Gaussian peak indicate its maximum value.

and Case 4), because then hardly any backscattered light interacts with the sea ice. However, for a thin snow layer (Case 2) the specular reflection component becomes important, and for $\phi = 0$ there is a significant discrepancy between CASIO-DISORT and ISBRDF. The cause of this discrepancy is that CASIO-DISORT includes diffuse light that has passed through the thin snow layer in near-forward directions and then undergone specular reflection [Eq. (2)], whereas ISBRDF without specular reflection [second term in Eq. (20)] does not include any interaction of the incident light with the air-ice interface. Figure 4 shows that the inclusion of a Gaussian specular reflection component leads to good agreement between ISBRDF and CAO-DISORT except for directions close to that of specular reflection. Note that CAO-DISORT does not include specular reflection of the direct beam, which explains the difference for directions close to that of specular reflection. CAO-DISORT does, however, include specular reflection of diffuse light, which explains the good agreement between CAO-DISORT and ISBRDF for angles off the specular direction (see Fig. 4).

To examine in more detail the effect of the snow thickness on the direct component of the specular reflection we gradually increased it from zero (bare ice) to 3 mm. Thus, in Fig. 5 we show a comparison of BRDF results computed with CASIO-DISORT and with ISBRDF for snow depths 0 (Case 1), 0.5 (Case 2), 1 (Case 3), 1.5 (Case 4), 2 (Case 5) and 3 (Case 6) mm. The results produced by the ISBRDF (broken lines) agree very well with the CASIO-DISORT results outside the specular reflection region. Recall that only the diffuse part of the specular reflection is included in CASIO-DISORT whereas ISBRDF includes both the diffuse and direct components. We also note that the direct component gradually becomes weaker as the snow thickness

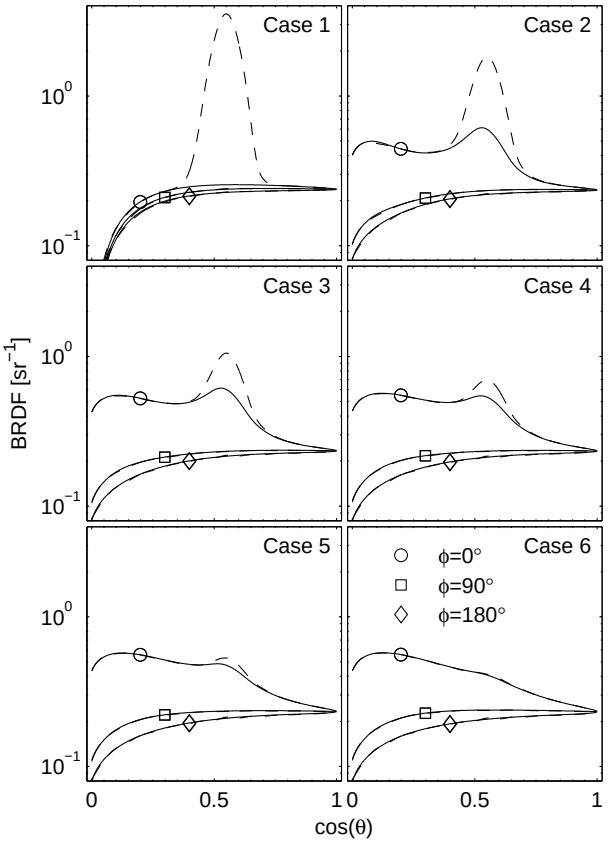

Figure 5. Comparison of BRDF results computed directly with CASIO-DISORT and with the ISBRDF package. Cases 1 through 6 correspond to snow layer thicknesses of 0 (bare ice), 0.5, 1, 1.5, 2, and 3 mm, respectively.

increases. For a snow thickness of 2 mm it is barely discernible, and for a snow thickness of 3 mm it has disappeared.

5. CONCLUSIONS

We have constructed a software tool for computing the BRDF for sea ice with and without snow cover as well as a new software tool for generating sea ice IOPs (single-scattering albedo, extinction optical depth, and scattering asymmetry parameter), for any wavelength between 300 nm and 4,000 nm as a function of sea ice physical parameters (real and imaginary parts of the sea ice refractive index, brine pocket concentration and effective brine pocket size, air bubble concentration and effective air bubble size, volume fraction of ice impurities and impurity absorption coefficient, asymmetry parameters for scattering by brine pockets and air bubbles, and sea ice thickness). The CASIO-DISORT code was used to compute LUTs of the Fourier expansion coefficients of the BRDF as a function of angles of illumination and observation, sea ice IOPs, and ocean albedo. By interpolation in the LUTs one efficiently obtains accurate BRDF values. To include snow on the ice we used DISORT2 (which allows for a BRDF to be used as a

lower boundary condition at the bottom of the atmosphere), appropriately modified to accept Fourier expansion coefficients for the BDRF as input instead of the BRDF itself, thereby reducing the computation time by a factor of about 60. The BRDF computed by CASIO-DISORT or retrieved from the LUTs applies to diffuse light only. To remedy this shortcoming we added a specular Gaussian beam component to the new BRDF tool and verified that it works well for BRDFs for bare and snow-covered sea ice.

REFERENCES

[1] Z. Jin, and K. Stamnes, "Radiative transfer in nonuniformly refracting media such as the atmosphere/ocean system," *Applied Optics*, **33**, 431-442 (1994).

[2] K. Stamnes, S.-C. Tsay, W.J. Wiscombe and K. Jayaweera, "Numerically stable algorithm for discrete-ordinate-method radiative transfer in multiple scattering and emitting layered media," *Applied Optics*, **27**, 2502-2509 (1988).

[3] K. Stamnes, S.-C. Tsay, W. J. Wiscombe and I. Laszlo, "DISORT, A General-Purpose Fortran Program for Discrete-Ordinate-Method Radiative Transfer in Scattering and Emitting Layered Media: Documentation of Methodology," Report, available from ftp://climate1.gsfc.nasa.gov/wiscombe/, 2000.

[4] G. E. Thomas and K. Stamnes, *Radiative Transfer in the Atmosphere and Ocean*, Cambridge University Press, New York & USA (1999).

[5] C. D. Mobley, B. Gentili, H. R. Gordon, Z. Jin, G. W. Kattawar, A. Morel, P. Reinersman, K. Stamnes, and R. H. Stavn, "Comparison of numerical models for computing underwater light fields," *Applied Optics*, **32**, 7484-7504 (1993).

[6] K. I. Gjerstad, J. J. Stamnes, B. Hamre, J. K. Lotsberg, B. Yan and K. Stamnes, "Monte Carlo and discrete-ordinate simulations of irradiances in the coupled atmosphere-ocean system," *Applied Optics*, **42**, 2609-2622 (2003).

[7] Z. Jin, K. Stamnes, W. F. Weeks, and S. C. Tsay, "The effect of sea ice on the solar energy budget in the atmosphere-sea ice-ocean system: A model study," *J. Geophys. Res.*, **99**, 25281-25294 (1994).

[8] C. F. Bohren, and D. R. Huffman, *Absorption and Scattering by Small Particles*, John Wiley, New York & USA (1983).

[9] B. Hamre, J.-G. Winther, S. Gerland, J. J. Stamnes, and K. Stamnes, "Modeled and measured optical transmittance of snow covered first-year sea ice in Kongsfjorden, Svalbard," *J. Geophys. Res.*, **109**, d0i:10.1029/2003JC001926 (2004).

[10] S. Jiang, K. Stamnes, W. Li and B. Hamre, "Enhanced Solar Irradiance Across the Atmosphere-Sea Ice Interface: A Quantitative Numerical Study," *Applied Optics*, **44**, 2613-2625 (2005).

[11] K. Stamnes, "Remote Sensing of the Environment: A Review of Forward-Modeling Requirements," in *Exploring the atmosphere by remote sensing*, R. Guzzi (Ed.), Springer Verlag (2003).

[12] K. Stamnes, W. Li, B. Yan, H. Eide, A. Barnard, W. S. Pegau and J. J. Stamnes, "Accurate and self-consistent ocean color algorithm: simultaneous retrieval of aerosol optical properties and chlorophyll concentrations," *Applied Optics*, **42**, 939-951 (2003).

[13] S. G. Warren, and R. E. Brandt, "Optical constants of ice from the ultraviolet to the microwave: A revised compilation," *J. Geophys. Res.*, **113**, D14220, doi:10.1029/2007JD009744 (2008).